molecular pharmaceutics

pubs.acs.org/molecularpharmaceutics

Article

Modeling of Particle Dissolution Behavior Using a Geometrical Phase-Field Approach

Dominik Sleziona, David R. Ely, and Markus Thommes*

Cite This: *Mol. Pharmaceutics* 2022, 19, 3749−3756

Read Online

ACCESS | Metrics & More | Article Recommendations

ABSTRACT: Material dissolution is a critical attribute of many products in a wide variety of industries. The idealized view of dissolution through established prediction tools should be reconsidered because the number of new substances with low aqueous solubility is increasing. Due to this, a fundamental understanding of the dissolution process is desired. The aim of this study was to develop a tool to predict crystal dissolution performance based on experimentally measurable physical parameters. A numerical simulation, called the phase-field method, was used to simultaneously solve the time evolution of the phase and concentration fields of dissolving particles. This approach applies to diffusion-limited as well as surface reaction-limited systems. The numerical results were compared to analytical solutions, and the influence of particle shape and interparticle proximity on the dissolution process was numerically investigated. Dissolution behaviors of two different substances were modeled. A diffusion-limited model compound, xylitol, with a high aqueous solubility and a surface reaction-limited model compound, griseofulvin, with a low aqueous solubility were chosen. The results of the simulations demonstrated that phase-field modeling is a powerful approach for predicting the dissolution behaviors of pure crystalline substances.

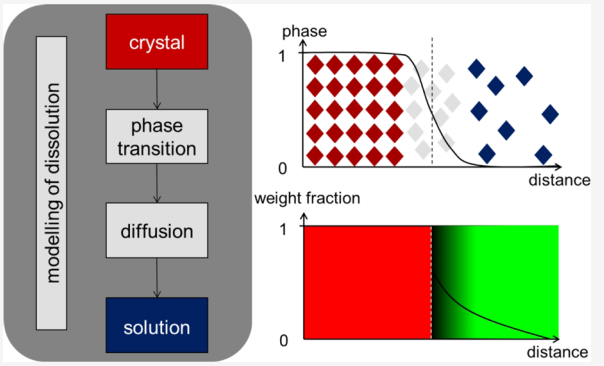

KEYWORDS: *diffusion, dissolution process, crystal, interface velocity, numerical model, surface reaction, phase-field simulation*

1. INTRODUCTION

The dissolution process is the basis of many process technologies ranging from synthesis to formulation and final performance. Modeling the dissolution process using conventional models is often insufficient when predicting the behavior of particles with nonspherical geometries, anisotropic systems, as well as clusters of particles in close proximity to each other or particle size distributions. Numerical approaches can be applied to overcome these limitations.

In this work, the phase-field method, which is a commonly used method for simulating phase boundaries (especially for metals), was adapted to simulate the dissolution of common pharmaceutical compounds in gently agitated systems. The method was compared to the Hixson−Crowell model and another analytical model derived for surface-reaction-limited substances to show consistency with well-established approaches, and additional capabilities of the phase-field method were demonstrated.

The phase-field method treats a solid−liquid system as a continuum and models the entire system, including the boundary between the two phases, as a scalar field in which the phase varies smoothly between perfectly ordered in the solid to perfectly disordered in the liquid.

The phase is described by a nonconserved order parameter (Φ), which is a function of space and time.[1−3] It is a continuous variable and ranges from a value of 0 in the liquid to a value of 1 in the solid. Figure 1a illustrates the continuous, smooth transition of the phase-field variable between the solid and liquid across the diffuse, solid−liquid interface. An advantage of this approach over sharp-interface models is the avoidance of a moving boundary at the interface, the so-called Stefan problem.[4,5]

In addition to modeling the phase, a multicomponent system requires that the concentration field also be accounted for, and indeed, the concentration field is directly coupled to the phase field. Herein, a binary system of a solute and a solvent is considered. As shown in Figure 1b, the diffusion process starts at the interface between the solid and liquid phases. Diffusion occurs in both directions—that is, from solute into the solvent as well as from liquid into the solid—

Received: March 22, 2022
Revised: August 23, 2022
Accepted: August 23, 2022
Published: September 6, 2022

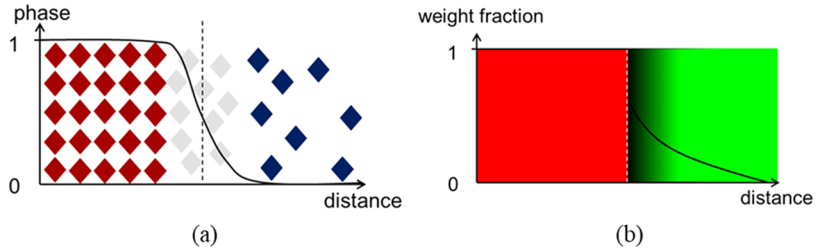

Figure 1. Graphical interpretation of the phase-field variable (a) and the diffusion process (b).

and is captured by the phase-field model. However, for the dissolution process of many crystalline materials in water, the diffusion of the water into the crystal can be neglected.

In this case, as the solid solute transforms into the liquid state through solvation, the solute then diffuses over time, t, into the solvent. In this paper, the concentration is expressed in terms of the weight fraction, which varies from zero (pure solvent) to one (pure solute). The link between diffusion and phase transition is the phase variable. As the solvent disrupts the crystal lattice of the solute at the interface, the resulting phase change across the diffuse interface is the source for the mass transport of the solute into the solvent. An advantage of this method is that no diffusion layer with sharp boundaries must be implemented, and modeling of the opposite phenomenon, crystallization, is possible as well using the same model.

In the literature, references with different focuses on the dissolution process can be found. It ranges from intrinsic dissolution experiments[6] of single crystal dissolution[7,8] to analytical equations for predicting dissolution process[9−17] and numerical models.[18−23] Nevertheless, the basis of these experiments, calculations, and models is the dissolution behavior of each single substance used for these formulations. However, previous work has shown that the dissolution behavior of drugs is not limited only by diffusion and convection. For some substances, the phase transition, or the surface reaction, is the limiting factor of the dissolution kinetics.[15,24]

In this work, the phase-field approach was used to describe the dissolution behavior of single, crystalline particles. The approach was compared to the Hixson−Crowell law for a diffusion-limited substance. For surface reaction-limited material, the phase-field simulation was compared to the analytical solution of a corresponding, derived equation. As a proof of concept, the ability of the phase-field method to be used to study systems beyond the scope of the Hixson−Crowell model, such as systems with nonspherical particles and clusters of particles, was also demonstrated.

2. MATERIALS

To ensure that the simulation captured a wide range of dissolution behavior, two model substances were chosen—one diffusion-limited substance (xylitol, Xylisorb 300, Roquette GmbH, Lestrem, France) and one surface reaction-limited substance (griseofulvin, Hawkins Inc., Roseville). Deionized water was used for surface tension and saturation concentration measurements.

3. METHODS

3.1. Numerical Setup. The simulation was performed in python 2.6.6 (Python Software Foundation, Wilmington) using the finite volume, partial differential equation solver, and Fipy 3.0.1.[25] A linear LU solver was used to simultaneously solve the partial differential equations used to model the system. All simulations were run on a DELL PowerEdge R720 computer (Dell Technologies Inc., Round Rock, TX) equipped with thirty-two, 2.00 GHz, Intel Xeon E5-2640 processor cores (Intel Corp., Santa Clara) and 64 GB of RAM. The total computational time took about 2 days for each dissolution simulation.

3.2. Interface Velocity. The interface velocity, v_n, is the speed and direction in which the interface moves during dissolution (or crystallization). Herein the interface velocity is defined as positive in the direction of growth and is given as the ratio of the surface reaction coefficient, k_{SR}, and the phase transition zone thickness, δ_{SR}.[26]

$$\frac{J_{SR}^{w}}{\rho_{solid} \cdot w_{solid}} = \frac{k_{SR}}{\delta_{SR}} = v_n \tag{1}$$

The interface velocity of the sugar alcohol, xylitol, and the substance, griseofulvin, was determined with dissolution experiments conducted in a laminar flow channel.[26] For each substance, deionized water (37 °C) was used and sink conditions were maintained ($w(t) < 0.1\ w_s$). Measurements were made in triplicate at four Reynolds numbers between 50 and 346, while the mass flux was determined from at least four data points. The surface reaction mass flux J_{SR}^{w} of griseofulvin was measured at four Reynolds numbers and used to calculate the interface velocity, v_n, using eq 1.

Since xylitol behaved as a highly diffusion-limited substance, no surface reaction mass flux was measurable. However, a pure diffusion mass flux J_{D}^{w} was used to estimate the minimum interface velocity of xylitol.

3.3. Melting Temperature and Enthalpy. Pure substance measurements were performed with differential scanning calorimetry (DSC Q2000, TA Instruments, New Castle). A sample size of approximately 10 mg was placed into a 40 μL aluminum pan. The cover of the pan was crimped with a punctured lid. The thermogram was recorded using heat rates of 1, 3, and 10 K·min^{-1}. The investigated sample was heated up from 223 to 413 K for xylitol and 273 to 523 K for griseofulvin, respectively. Three repetitions were performed for each measurement. The melting temperatures and enthalpies were extrapolated to 0 K·min^{-1} heating rate and used in subsequent calculations.

3.4. Free Surface Energy. Deionized water as a polar fluid and methylene iodide as a nonpolar fluid were used to measure the static contact angles between these fluids and the two model compounds, xylitol and griseofulvin. For each compound, 10 biplane tablets with a diameter of 5 mm and a weight of 300 ± 10 mg were produced. A single punch press (EK0, Korsch AG, Berlin, Germany) with a force of 5, 10, 15,

https://doi.org/10.1021/acs.molpharmaceut.2c00214
Mol. Pharmaceutics 2022, 19, 3749−3756

20, and 25 kN was used. A drop of each fluid was placed by the drop shape analyzer (G40, Krüss GmbH, Hamburg, Germany) on the surface, and the contact angle was measured automatically after 1 second by the Krüss analysis software. Based on the contact angle measurements from both liquids, the surface tension between the solid substances and water was calculated via the Young equation and the model from Owens and Wendt.[27]

3.5. Saturation Concentration and Slope of the Liquidus Line. The saturation concentrations of xylitol and griseofulvin were measured at dissolution temperatures of 293, 303, 310, 318, and 323 K. First, a supersaturated solution of the model compound powder in water was created. The solution was then stored for 48 h at the corresponding temperature. Samples, $n = 3$ per temperature and substance, were taken and filtered using a 0.45 μm syringe filter. All samples were diluted with deionized water to reach the corresponding calibration region. Using the refraction index, the concentration of xylitol samples could be determined with a refractometer (90204, Carl Zeiss AG, Oberkochen, Germany). The adsorption of griseofulvin was measured with a UV/Vis spectrometer (Biomate 3, Thermo Fischer Scientific, Waltham). Afterward, the saturation concentration and the slope of the liquidus line[28] could be calculated. However, due to its low aqueous solubility, the measured slope of the liquidus line from griseofulvin could only be determined for a narrow concentration range. The experimentally measured and calculated simulation parameters used are summarized in Table 1.

Table 1. Experimental and Calculated Simulation Parameters for Xylitol, Griseofulvin, and Water

parameter	xylitol	griseofulvin
molar volume [$m^3 \cdot mol^{-1}$]	1.00×10^{-4}	2.52×10^{-4}
melting temperature [K]	366	489
melting enthalpy [J g^{-1}]	256	96.04
system temperature [K]	310	
diffusion coefficient[a] [$m^2 \cdot s^{-1}$]	9.63×10^{-10}	7.09×10^{-10}
surface tension solid/water [$J \cdot m^{-2}$]	1.02×10^{-2}	1.86×10^{-2}
interfacial thickness [m]	5.5×10^{-9}	1.0×10^{-9}
slope of the liquidus line [K]	97.96	3.58×10^{7}
solubility [−]	0.80	2.18×10^{-5}
interface velocity [$m \cdot s^{-1}$]	-5.85×10^{-7}	-5.25×10^{-10}
Sherwood number[a] [−]	0.95	79

[a]Calculated via Stokes−Einstein equation[29] and Sherwood correlations.[30,31]

4. RESULTS AND DISCUSSION

4.1. Theoretical Framework. The dissolution process is divided into two parts. The crystal must first undergo a phase transition from the solid state into the liquid state, which occurs through the disruption of the crystal lattice at the interface by the solvent molecules. As the solvent diffuses into the disrupted lattice, the liquefied solute then diffuses into the surrounding solvent. Convection, if present, increases the mass transport in the solvent. The phase transition can be simulated numerically with the phase-field method.[2]

Previous investigations found in the literature modeled spinodal decomposition of alloys.[32−34] Here, pure substances as well as multicomponent systems were examined.[35] Besides this, the phase-field method is mainly used in materials science to investigate solidification processes in metal melts and alloys. Beckermann et al. presented a model for simulating the microstructural evolution during solidification in binary alloys by incorporating convection in the liquid melt. Here, the evolution equation of the phase field was derived using a geometrical approach based on the Gibbs−Thomson equation. In contrast, Boettinger et al.[2] derived the phase evolution equation using a thermodynamic description based on the continuum equations from Allen−Cahn and Cahn−Hilliard.[33,36] This model is used in many works to model phenomena such as solute trapping,[37] dendritic growth,[38] eutectic two-phase cell formation,[39] and formation of equiaxed dendritic grain structure.[40] Zhou and Powell[41] simulated polymer membrane phase separation during immersion precipitation using a ternary Cahn−Hilliard model in which the homogeneous Flory−Huggins energy function was implemented. The calculated two- and three-D models provide deeper insight into the immersion precipitation process.

In pharmaceutical materials science, however, the very promising phase-field approach is not yet well established as a useful tool despite its very powerful capabilities demonstrated in other fields.[42] One of the very few pharmaceutics examples is work published by Saylor et al.[21] in 2007, wherein the release behavior of controlled drug-release systems was modeled. In this work, a three-component system consisting of a solvent, drug, and polymer was modeled based on the thermodynamic approach described in Boettinger's review.[2]

Existing analytical approaches for the description of crystal dissolution like Fick's laws of diffusion, the Noyes−Whitney equation, the Hixson−Crowell cubic root law, and the Higuchi equation have been widely used in pharmaceutics.[43,44] However, they do not account for particle shape, proximity to other particles, or surface reaction effects. This was addressed using the phase-field method within this study.

The physical basis of the dissolving process for a crystal is cooling curves, originally used for phase diagram construction, which can be calculated by the Gibbs free energy of mixing. Phase-transformation processes such as melting or crystallization are driven by the change in free energy.[45] The conditions required for this are defined by the current state of the system and its equilibrium state, where the equilibrium state is characterized by the minimum of the free energy functional of the system.[45,46]

According to Beckermann,[1] the Gibbs−Thomson equation for an isotropic, binary system can be used. Normally this relation is utilized to describe a local thermodynamic equilibrium at the interface. However, during dissolution, the evolution of the phase in space and time means this is a nonequilibrium process, so a kinetic term must be included.[46] This kinetic term accounts for the movement of the interface during dissolution and is characterized by the interface velocity, v_n. From Beckermann's description, the phase evolves as

$$\frac{\partial \Phi}{\partial t} = v_n |\nabla \Phi| \tag{2}$$

The interface velocity is given by

$$v_n = \mu_k \left[T_m - T - m_l \frac{w}{1 - \Phi + k\Phi} - \Gamma \kappa \right] \tag{3}$$

Here, μ_k is the interface mobility, $T_m - T$ is the constitutional undercooling where T_m is the melting temperature of the pure

https://doi.org/10.1021/acs.molpharmaceut.2c00214
Mol. Pharmaceutics 2022, 19, 3749−3756

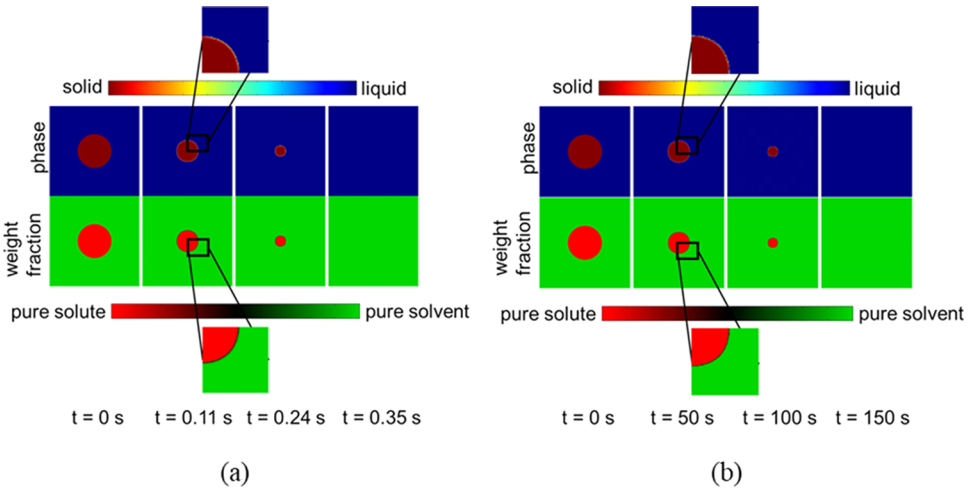

Figure 2. Selection of time points of the phase and weight fraction profile of a circular, isotropic, 150 nm starting diameter, diffusion-limited (a) and surface reaction-limited (b) crystal in water (Re = 100, ϑ = 37 °C).

substance and T is the temperature of the system, m_l is the slope of the liquidus line, Φ is the phase order parameter, w is the averaged weight fraction, k is the partition coefficient, Γ is the Gibbs–Thomson coefficient, and κ is the curvature of the interface. Expanding the curvature leads to the extended phase-field expression

$$\frac{\partial \Phi}{\partial t} = \mu_k \Gamma \left(-\nabla^2 \Phi + \frac{\Phi(1-\Phi)(1-2\Phi)}{\delta_{SR}^2} \right) + \mu_k \left(T_m - T - m_l \frac{w}{1-\Phi+k\Phi} \right) \frac{\Phi(1-\Phi)}{\delta_{SR}} \tag{4}$$

Here, δ_{SR} is the characteristic thickness of the interface. The phase change over space and time is related to the interface mobility μ_k, as well as an interfacial tension term that opposes the phase change. The description given by eq 4 gives rise to a smooth but well-defined interface with the thickness δ_{SR}. The second term of eq 4 is the thermal driving term and is the counterpart to the interfacial tension term. It forces the solid to change its phase due to the undercooling in the system.[46]

In the dissolution process, the phase change over space and time is coupled to the concentration field. In Beckermann's approach, the continuity equation for a multicomponent mixture[47] is used

$$\frac{\partial w}{\partial t} + \nabla \cdot \left(\frac{(1-\Phi)}{(1-\Phi)+k\Phi} v_L w \right) = \nabla \cdot \tilde{D} \left[\nabla w + \frac{(1-k)w}{(1-\Phi)+k\Phi} \nabla \Phi \right] \tag{5}$$

This equation shows the temporal change in concentration over space, and time is a function of a convection term, $\nabla \cdot \left(\frac{(1-\Phi)}{(1-\Phi)+k\Phi} v_L w \right)$, where v_L is the velocity of the fluid and w is the mass fraction of the solute, and a diffusion term, $\nabla \cdot \tilde{D} \left[\nabla w + \frac{(1-k)w}{(1-\Phi)+k\Phi} \nabla \Phi \right]$, where the $\tilde{D}$ is the phase averaged diffusivity. The diffusion term is a function of the gradient of the concentration field, ∇w (Fickian diffusion), and the gradient of the phase field, $\nabla \Phi$, which is the driving force for diffusion caused by the phase gradient across the solid–liquid interface.

Since the velocity vector field was not resolved in this work, the velocity of the fluid, v_L, was set to zero. Instead, the mass transport due to convection was modeled in terms of an effective diffusion term, $\tilde{D}Sh\nabla w$, where Sh is the Sherwood number. This term was added to the Fickian diffusion term, $\tilde{D}\nabla w$, leading to

$$\frac{\partial w}{\partial t} = \nabla \cdot \tilde{D} \left[(1+Sh)\nabla w + \frac{(1-k)w}{(1-\Phi)+k\Phi} \nabla \Phi \right] \tag{6}$$

The advantage is that the influence of convection on the dissolution process can be approximated without knowing the velocity vector field of the fluid. The diffusive flux can be understood as a sink or source term that is directly related to the surface reaction accounted for by the term $\frac{(1-k)w}{(1-\Phi)+k\Phi} \nabla \Phi$. Via this term, eq 6 is coupled to eq 4, which governs the evolution of the phase field. It is noted here that eqs 4 and eq 6 are geometrical descriptions that correspond to the Allen–Cahn and Cahn–Hilliard equations, respectively, explained in detail by Boettinger.[2] In eqs 4 and eq 6, all critical simulation parameters could be experimentally measured or calculated via well-established methods and relations (see Table 1).

4.2. Comparison of Phase-Field Simulation. Initial investigations were conducted to compare the phase-field results to analytical solutions. Dissolution experiments in the flow channel (see Section 3.2) indicated diffusion-limited dissolution behavior for xylitol, so xylitol was chosen as a model compound because its dissolution behavior is readily described by the Hixson–Crowell cube root law given by

$$m_0^{1/3} - m_R^{1/3} = \frac{D(c_s - c)}{\delta_D} \cdot \frac{(4\pi/3)^{1/3}}{\rho_s^{2/3}} \cdot t \tag{7}$$

Here, the remaining particle mass, m_R, is a function of the initial particle mass, m_0, the diffusion coefficient, D, the diffusion layer thickness, δ_D, the density of the solute, ρ_s, and the dissolution time, t. However, eq 7 assumes a spherical particle, the three-dimnsional (3D) nature of which requires considerably higher computing resources. However, as this was a preliminary study, a two-dimensional version of the law was derived for an isotropic cylinder that dissolved only over its

https://doi.org/10.1021/acs.molpharmaceut.2c00214
Mol. Pharmaceutics 2022, 19, 3749–3756

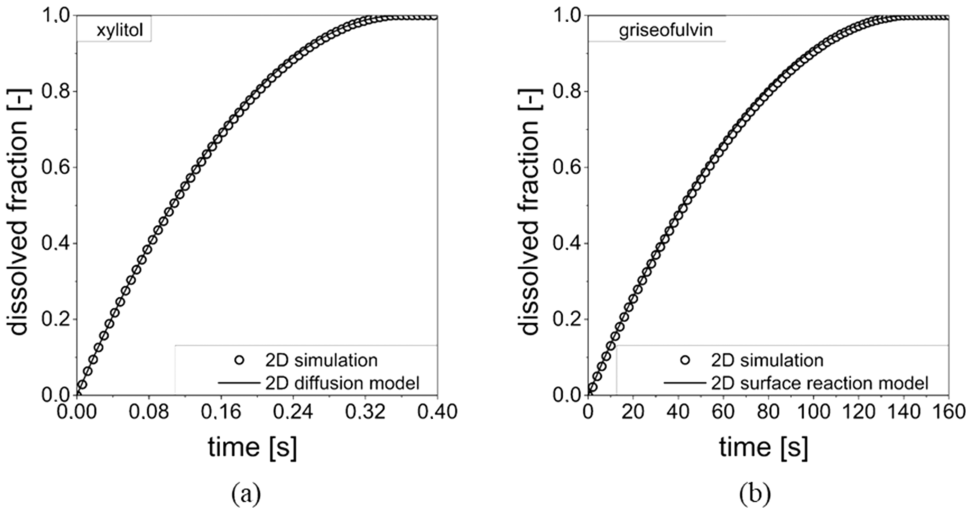

Figure 3. Dissolved fraction of a circular, isotropic, 150 nm starting diameter, diffusion-limited particle (a) and surface reaction-limited (b) crystal in agitated water (Re = 100, ϑ = 37 °C) as a function of time. Simulated data using the phase-field method (○) are shown in conjunction with the analytical model results (−). The 2D diffusion model was compared to xylitol, and the 2D surface reaction model was compared to griseofulvin.

lateral surface. This is more easily simulated since the cylinder is equivalent to a circle in the simulation. The main advantage of this is the much faster computational time along with a simple, homogeneous, and reproducible mesh. The obtained numerical model can be expanded with little effort. Accordingly, in two dimensions, the Hixson−Crowell law reduces to

$$d = d_0 - \frac{2 \cdot D \cdot w_s}{\delta_D} \cdot t \tag{8}$$

The resulting equation describes a cylinder dissolved under sink conditions over its lateral surface and is referred to herein as the two-dimensional (2D) diffusion model. Here, the remaining particle diameter, d, is a function of the initial diameter, d_0, the diffusion coefficient, and the solubility limit in terms of the weight fraction, w_s.

A corresponding equation had to be derived for the poorly soluble, surface reaction-limited compound. This equation must describe the reduction of the particle diameter over time due to the kinetics of the surface reaction. Using the interface velocity given by eq 1, eq 8 can be rewritten for surface reaction-limited compounds as

$$d = d_0 - \frac{2 \cdot k_{SR} \cdot w_{solid}}{\delta_{SR}} \cdot t = d_0 - 2 \cdot \nu_n \cdot w_{solid} \cdot t \tag{9}$$

This model is referred to herein as the 2D surface reaction model. The analytical solutions of these well-known analytical models were compared to the results from the numerical simulations.

Figure 2 shows the corresponding phase and concentration fields for a single particle of xylitol and griseofulvin dissolving in water. Here, an isotropic, circular, two-dimensional, slightly agitated particle, with an initial diameter of 150 nm, dissolving in water at 37 °C was simulated. The simulation space was 400 × 400 nm, and the midpoint of the particle was initialized at the center.

A simultaneously evolving phase field and concentration field could be observed. The pure, solid-state crystal is represented by a phase and mass fraction of 1 (red). The phase transitions smoothly, albeit rapidly, over a transition zone from the solid state to the liquid state, which is represented by a phase value of 0 (blue). The transition zone can be observed in Figure 2 as a thin, light-colored ring around the red particle.

The diffusion (eq 6) is coupled to the phase reaction (eq 4), so as the solid liquifies across the transition zone, the mobility of the solute dramatically increases, resulting in rapid diffusion into the solvent. Based on the Dirichlet (fixed value) boundary conditions[45] of w = 0 at the edges of the domain, the dissolved solute was rapidly transported out of the system. This can be seen in Figure 2, where red corresponds to pure solute (w = 1) and green corresponds to pure solvent (w = 0). The thin, dark ring around the particle in the concentration fields corresponds to the transition zone where the diffusivity and convection dramatically increase leading to rapid mass transport from the surface of the particle into the solvent and out of the system across the boundaries of the domain. As the simulation progressed, the particle shrank. That is, the transition zone of the phase field receded toward the center of the particle with the concentration field tracking closely.

Figure 3 shows the plotted dissolved fraction of the particle diameter from a phase-field simulation as a function of the simulated time. Simulation results for xylitol were in excellent agreement with the 2D diffusion model (eq 8) for xylitol (Figure 3a). The total dissolution time of the simulated 150 nm diameter xylitol particle was 0.35 s.

To validate the presented phase-field simulation, a model substance that exhibited surface reaction-limited dissolution behavior was needed. Previous work by the authors demonstrated that the substance griseofulvin met this requirement.[26] A relatively sharp interface between the solid and liquid was required for this substance, so an interfacial thickness of 1 nm corresponding to the spatial resolution of the simulation was used. This is consistent with the hydrophobic behavior of griseofulvin since it implies a very limited ability of the solvent to penetrate the crystal.[48] Excellent agreement with the 2D surface reaction model (eq 9) was observed. The total dissolution time of the simulated 150 nm diameter griseofulvin particle was 140 s.

4.3. Influence of Particle Shape on Dissolution Process. The first application of the phase-field simulations

https://doi.org/10.1021/acs.molpharmaceut.2c00214
Mol. Pharmaceutics 2022, 19, 3749−3756

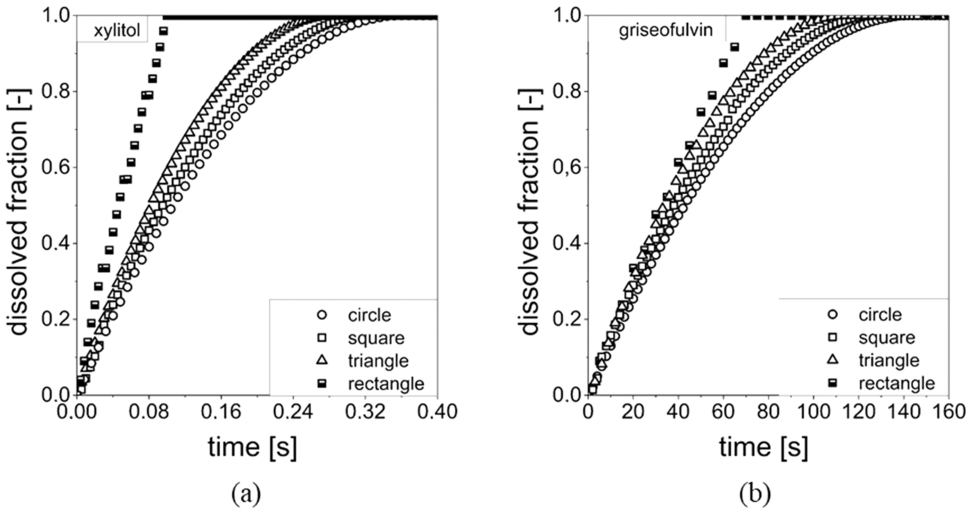

Figure 4. Simulation results showing dissolved fraction as a function of time of circular, triangular, square, and rectangular isotropic particles for diffusion-limited (a) and surface reaction-limited (b) crystals in agitated water (Re = 100, ϑ = 37 °C).

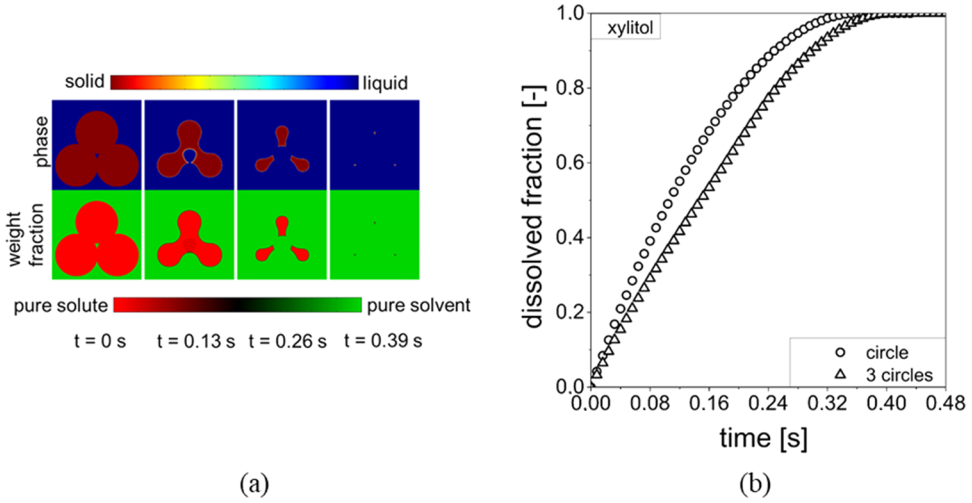

Figure 5. Selection of time points of the phase and weight fraction profile (a) and dissolved fraction (b) of diffusion-limited crystals in close proximity in agitated water (Re = 100, ϑ = 37 °C).

presented herein is the investigation of the influence of particle shape with respect to the dissolution kinetics under the aforementioned simulation conditions (see Section 4.2). For both substances—diffusion-limited xylitol and surface reaction-limited griseofulvin—a square, an equilateral triangle, and a rectangle with an aspect ratio of 5:1 were initialized.

Figure 4 shows the dissolved fraction as a function of the simulated dissolution time of these particles. The differently shaped particles were initialized to have an equivalent initial area equal to the initial area of the 150 nm starting diameter, circular particles in the comparison experiments (see Section 4.2). It could be observed that the dissolution time reduced with increasing initial circumference for both substances. The rectangular particle especially exhibited a significantly lower total dissolution time. Compared to the circular particles, the rectangular particle dissolved 1.8 times faster for the diffusion-limited compound and 1.2 times faster for the surface reaction-limited compound. Dissolution occurred predominantly along the long sides of the rectangles.

4.4. Influence of Interparticle Proximity on the Dissolution Process. The second application of phase-field simulation is the investigation of the influence of interparticle proximity on dissolution kinetics. In other words, how does placing particles in close proximity to each other influence the dissolution process? For both model compounds, three partially overlapping, circular particles were simulated and compared to the results of the corresponding single particle.

The results for xylitol are shown in Figure 5. Initially, the single particle dissolves more quickly than the three overlapping particles. However, the dissolution curves converge toward the end of the dissolution processes resulting in similar total dissolution times. The retarded dissolution kinetics of the multiparticle system can be explained due to the lower amount of exposed interface between the solid and solvent. A change in particle shape was also observed in which the concave corners evolved to form a smooth envelope encompassing all three particles. This change is driven by the system reducing its total surface free energy by reducing the total interfacial area.

The phase field also shows that the surface of the particles forming the interstice between the three particles began to dissolve, and the concentration increased in the trapped solvent until the necks between adjacent particles pinched off

https://doi.org/10.1021/acs.molpharmaceut.2c00214
Mol. Pharmaceutics 2022, 19, 3749−3756

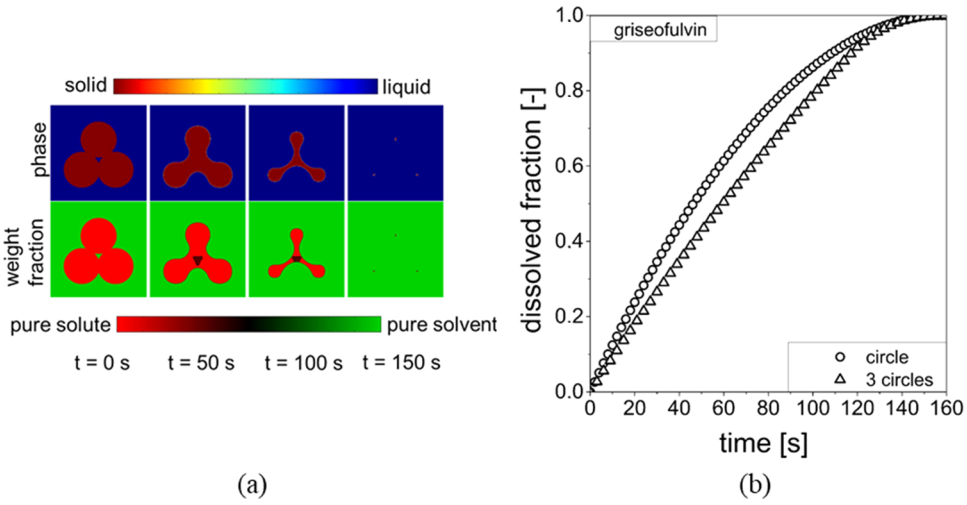

Figure 6. Selection of time points of the phase and weight fraction profile (a) and dissolved fraction (b) of surface reaction-limited crystals in close proximity in agitated water (Re = 100, ϑ = 37 °C).

exposing the interstice to the bulk solvent. Once the shielded interior was exposed, the now separate particles rapidly dissolved with no interference from each other.

For the surface reaction-limited compound, griseofulvin, a smooth envelope formed around the three particles in the same manner as observed with the xylitol particles, but a different effect was observed in the interstitial region (Figure 6). At the center of the structure (interstice), the solvent supersaturated and solidified.

Similar to xylitol, the dissolution kinetics of the three-particle system were also initially retarded for griseofulvin in comparison to a single particle but converged with the single-particle dissolution profile resulting in a very similar total dissolution time.

These simulations demonstrate that the phase-field method is a versatile tool that can predict the dissolution process of different particle shapes for both diffusion-limited and surface reaction-limited substances. Additionally, it can also be used to investigate the effect of interparticle proximity on dissolution kinetics.

5. CONCLUSIONS

A phase-field method was developed to investigate the dissolution behavior of crystalline particles in which all critical parameters could be determined. The dissolution behavior of circular, isotropic crystals in water at 37 °C was simulated for two substances—a diffusion-limited compound and a surface reaction-limited compound. Excellent agreement of the phase-field simulations with derived analytical models was observed.

Additionally, the influence of the particle shape and interparticle proximity was investigated. As expected, the dissolution time depended on the initial circumference of both substances. Also, it was demonstrated that dissolution effects resulting from solvent inclusions and shape changes during the dissolution process could be investigated using the phase-field method.

This technique of modeling the dissolution behavior of crystalline substances is a powerful tool to investigate both diffusion-limited and surface reaction-limited dissolution behavior. Additionally, as a numerical approach, it can be readily extended to investigate the dissolution behavior of particle size distributions, more complex particle shapes, anisotropy, and multicomponent formulations.

AUTHOR INFORMATION

Corresponding Author

Markus Thommes − *TU Dortmund, Department of Biochemical and Chemical Engineering, Laboratory of Solids Process Engineering, 44227 Dortmund, Germany;* orcid.org/0000-0002-6217-9902; Email: professors.fsv.bci@tu-dortmund.de

Authors

Dominik Sleziona − *TU Dortmund, Department of Biochemical and Chemical Engineering, Laboratory of Solids Process Engineering, 44227 Dortmund, Germany;* orcid.org/0000-0003-0465-6763

David R. Ely − *Ivy Tech Community College, Lafayette, Indiana 47905, United States*

Complete contact information is available at: https://pubs.acs.org/10.1021/acs.molpharmaceut.2c00214

Author Contributions

The manuscript was written through contributions of all authors. All authors have given approval to the final version of the manuscript.

Notes

The authors declare no competing financial interest.

ACKNOWLEDGMENTS

The authors are grateful for the financial support of the DECHEMA e.V. ProcessNet section Agglomeration and Bulk Material Technology.

SYMBOLS

c, bulk concentration (kg·m^{-3}); c_s, saturation concentration (kg·m^{-3}); D, diffusivity (m^2·s^{-1}); $\tilde{D}$, phase averaged diffusivity (m^2·s^{-1}); d, particle diameter (m); d_0, initial particle diameter (m); J_D^w, diffusion mass flux (kg·m^{-2}·s^{-1}); J_{SR}^w, surface reaction mass flux (kg·m^{-2}·s^{-1}); k, partition coefficient; k_{SR}, surface reaction coefficient (m^2·s^{-1}); m_0, initial mass (kg); m_l, slope of the liquidus line (K); m_R, remaining mass (kg); Sh, Sherwood number; T, temperature (K); T_m, melting temperature (K); t,

https://doi.org/10.1021/acs.molpharmaceut.2c00214
Mol. Pharmaceutics 2022, 19, 3749−3756

time (s); v_n, normal interface velocity ($m \cdot s^{-1}$); v_L, velocity of the fluid ($m \cdot s^{-1}$); w, weight fraction ($kg \cdot kg^{-1}$); w_s, weight fraction at the solubility limit ($kg \cdot kg^{-1}$); w_{solid}, weight fraction of the solid ($kg \cdot kg^{-1}$); Γ, Gibbs−Thomson coefficient ($m \cdot K$); δ_D, diffusion layer thickness (m); δ_{SR}, interfacial thickness (m); κ, curvature (m); μ_k, linear kinetic coefficient ($K \cdot s \cdot m^{-1}$); ρ_s, density of the solute ($kg \cdot m^{-3}$); ρ_{solid}, density of the solid ($kg \cdot m^{-3}$); Φ, phase; ϑ, temperature (°C)

REFERENCES

(1) Beckermann, C.; Diepers, H.-J.; Steinbach, I.; Karma, A.; Tong, X. Modeling melt convection in phase-field simulations of solidification. *J. Comput. Phys.* **1999**, *154*, 468−496.

(2) Boettinger, W. J.; Warren, J. A.; Beckermann, C.; Karma, A. Phase-Field Simulation of Solidification. *Annu. Rev. Mater. Res.* **2002**, *32*, 163−194.

(3) Cui, Z.; Gao, F.; Cui, Z.; Qu, J. Developing a second nearest-neighbor modified embedded atom method interatomic potential for lithium. *Modell. Simul. Mater. Sci. Eng.* **2012**, *20*, No. 15014.

(4) Gupta, S. C. *The Classical Stefan Problem: Basic Concepts, Modelling and Analysis with Quasi-Analytical Solutions and Methods*, Elsevier: 2017.

(5) Meirmanov, A. M. *The Stefan problem, volume 3 of de Gruyter Expositions in Mathematics*, Walter de Gruyter & Co.: Berlin, 1992.

(6) Yu, L. X.; Carlin, A. S.; Amidon, G. L.; Hussain, A. S. Feasibility studies of utilizing disk intrinsic dissolution rate to classify drugs. *Int. J. Pharm.* **2004**, *270*, 221−227.

(7) Prasad, K. V. R.; Ristic, R. I.; Sheen, D. B.; Sherwood, J. N. Dissolution kinetics of paracetamol single crystals. *Int. J. Pharm.* **2002**, *238*, 29−41.

(8) Svanbäck, S.; Ehlers, H.; Yliruusi, J. Optical microscopy as a comparative analytical technique for single-particle dissolution studies. *Int. J. Pharm.* **2014**, *469*, 10−16.

(9) Brunner, E. Reaktionsgeschwindigkeit in heterogenen Systemen. *Z. Phys. Chem.* **1904**, *47*, 56−102.

(10) Craig, D. Q. M. The mechanisms of drug release from solid dispersions in water-soluble polymers. *Int. J. Pharm.* **2002**, *231*, 131−144.

(11) Dokoumetzidis, A.; Papadopoulou, V.; Valsami, G.; Macheras, P. Development of a reaction-limited model of dissolution: Application to official dissolution tests experiments. *Int. J. Pharm.* **2008**, *355*, 114−125.

(12) Fick, A. Ueber diffusion. *Ann. Phys.* **1855**, *170*, 59−86.

(13) Higuchi, T. Rate of release of medicaments from ointment bases containing drugs in suspension. *J. Pharm. Sci.* **1961**, *50*, 874−875.

(14) Hixson, A. W.; Crowell, J. H. Dependence of Reaction Velocity upon Surface and Agitation. *Ind. Eng. Chem.* **1931**, *23*, 1160−1168.

(15) Ji, Y.; Paus, R.; Prudic, A.; Lübbert, C.; Sadowski, G. A novel approach for analyzing the dissolution mechanism of solid dispersions. *Pharm. Res.* **2015**, *32*, 2559−2578.

(16) Nernst, W. Theory of reaction velocity in heterogenous systems. *Z. Phys. Chem.* **1904**, *47*, 52−55.

(17) Siepmann, J.; Göpferich, A. Mathematical modeling of bioerodible, polymeric drug delivery systems. *Adv. Drug Delivery Rev.* **2001**, *48*, 229−247.

(18) Wang, Y.; Abrahamsson, B.; Lindfors, L.; Brasseur, J. G. Analysis of Diffusion-Controlled Dissolution from Polydisperse Collections of Drug Particles with an Assessed Mathematical Model. *J. Pharm. Sci.* **2015**, *104*, 2998−3017.

(19) Wang, Y.; Abrahamsson, B.; Lindfors, L.; Brasseur, J. G. Comparison and analysis of theoretical models for diffusion-controlled dissolution. *Mol. Pharmaceutics* **2012**, *9*, 1052−1066.

(20) Chen, Q.; Ma, N.; Wu, K.; Wang, Y. Quantitative phase field modeling of diffusion-controlled precipitate growth and dissolution in Ti−Al−V. *Scr. Mater.* **2004**, *50*, 471−476.

(21) Saylor, D. M.; Kim, C.-S.; Patwardhan, D. V.; Warren, J. A. Diffuse-interface theory for structure formation and release behavior in controlled drug release systems. *Acta Biomater.* **2007**, *3*, 851−864.

(22) Wang, G.; Xu, D. S.; Ma, N.; Zhou, N.; Payton, E. J.; Yang, R.; Mills, M. J.; Wang, Y. Simulation study of effects of initial particle size distribution on dissolution. *Acta Mater.* **2009**, *57*, 316−325.

(23) Yang, S.; Ukrainczyk, N.; Caggiano, A.; Koenders, E. Numerical Phase-Field Model Validation for Dissolution of Minerals. *Appl. Sci.* **2021**, *11*, 2464.

(24) Paus, R.; Ji, Y.; Braak, F.; Sadowski, G. Dissolution of Crystalline Pharmaceuticals: Experimental Investigation and Thermodynamic Modeling. *Ind. Eng. Chem. Res.* **2015**, *54*, 731−742.

(25) Guyer, J. E.; Wheeler, D.; Warren, J. A. FiPy: Partial differential equations with Python. *Comput. Sci. Eng.* **2009**, *11*, 6−15.

(26) Sleziona, D.; Mattusch, A.; Schaldach, G.; Ely, D. R.; Sadowski, G.; Thommes, M. Determination of Inherent Dissolution Performance of Drug Substances. *Pharmaceutics* **2021**, *13*, 146.

(27) Owens, D. K.; Wendt, R. C. Estimation of the surface free energy of polymers. *J. Appl. Polym. Sci.* **1969**, *13*, 1741−1747.

(28) Porter, D. A.; Easterling, K. E. *Phase Transformations in Metals and Alloys*, 2nd ed., reprinted.; Chapman & Hall, 1992.

(29) Einstein, A. Über die von der molekularkinetischen Theorie der Wärme geforderte Bewegung von in ruhenden Flüssigkeiten suspendierten Teilchen. *Ann. Phys.* **1905**, *322*, 549−560.

(30) Brauer, H.; Mewes, D. *Stoffaustausch einschließlich chemischer Reaktionen*; Sauerländer, 1971.

(31) Pohlhausen, E. Der Wärmeaustausch zwischen festen Körpern und Flüssigkeiten mit kleiner Reibung und kleiner Wärmeleitung. *Z. Angew. Math. Mech.* **1921**, *1*, 115−121.

(32) Cahn, J. W. On spinodal decomposition. *Acta Metall.* **1961**, *9*, 795−801.

(33) Cahn, J. W.; Hilliard, J. E. Free Energy of a Nonuniform System. I. Interfacial Free Energy. *J. Chem. Phys.* **1958**, *28*, 258−267.

(34) Hillert, M. H. *A Theory of Nucleation for Solid Metallic Solutions*; Massachusetts Institute of Technology, 1956.

(35) Singer-Loginova, I.; Singer, H. M. The phase field technique for modeling multiphase materials. *Rep. Prog. Phys.* **2008**, *71*, No. 106501.

(36) Allen, S. M.; Cahn, J. W. A microscopic theory for antiphase boundary motion and its application to antiphase domain coarsening. *Acta Metall.* **1979**, *27*, 1085−1095.

(37) Aziz, M. J. Model for solute redistribution during rapid solidification. *J. Appl. Phys.* **1982**, *53*, 1158−1168.

(38) Ely, D. R.; Jana, A.; García, R. E. Phase field kinetics of lithium electrodeposits. *J. Power Sources* **2014**, *272*, 581−594.

(39) Plapp, M.; Karma, A. Eutectic colony formation: a phase-field study. *Phys. Rev. E* **2002**, *66*, 61608.

(40) Kobayashi, R. A Numerical Approach to Three-Dimensional Dendritic Solidification. *Exp. Math.* **1994**, *3*, 59−81.

(41) Zhou, B.; Powell, A. C. Phase field simulations of early stage structure formation during immersion precipitation of polymeric membranes in 2D and 3D. *J. Membr. Sci.* **2006**, *268*, 150−164.

(42) Prajapati, N.; Späth, M.; Knecht, L.; Selzer, M.; Nestler, B. Quantitative Phase-Field Modeling of Faceted Crystal Dissolution Processes. *Cryst. Growth Des.* **2021**, *21*, 3266−3279.

(43) Siepmann, J.; Siepmann, F. Mathematical modeling of drug dissolution. *Int. J. Pharm.* **2013**, *453*, 12−24.

(44) Siepmann, J.; Siepmann, F. Modeling of diffusion controlled drug delivery. *J. Controlled Release* **2012**, *161*, 351−362.

(45) Balluffi, R. W.; Allen, S.; Carter, W. C. *Kinetics of Materials*; John Wiley & Sons, 2005.

(46) Stefanescu, D. M. *Science and Engineering of Casting Solidification*; Springer, 2015.

(47) Bird, R. B.; Stewart, W. E.; Lightfoot, E. N. *Transport Phenomena*; John Wiley & Sons: New York, 1960; Vol. *413*.

(48) Thommes, M.; Ely, D. R.; Carvajal, M. T.; Pinal, R. Improvement of the Dissolution Rate of Poorly Soluble Drugs by Solid Crystal Suspensions. *Mol. Pharmaceutics* **2011**, *8*, 727−735.

https://doi.org/10.1021/acs.molpharmaceut.2c00214
Mol. Pharmaceutics 2022, 19, 3749−3756